

The effect of soil improvement and auxiliary rails at railway track transition zones

Chumyen, P. ; Connolly, D.P. ; Woodward, P.K. ; Markine, V.

DOI

[10.1016/j.soildyn.2022.107200](https://doi.org/10.1016/j.soildyn.2022.107200)

Publication date

2022

Document Version

Final published version

Published in

Soil Dynamics and Earthquake Engineering

Citation (APA)

Chumyen, P., Connolly, D. P., Woodward, P. K., & Markine, V. (2022). The effect of soil improvement and auxiliary rails at railway track transition zones. *Soil Dynamics and Earthquake Engineering*, 155, 1-9. Article 107200. <https://doi.org/10.1016/j.soildyn.2022.107200>

Important note

To cite this publication, please use the final published version (if applicable). Please check the document version above.

Copyright

Other than for strictly personal use, it is not permitted to download, forward or distribute the text or part of it, without the consent of the author(s) and/or copyright holder(s), unless the work is under an open content license such as Creative Commons.

Takedown policy

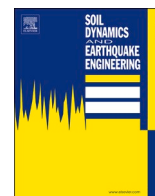
Please contact us and provide details if you believe this document breaches copyrights. We will remove access to the work immediately and investigate your claim.

Green Open Access added to TU Delft Institutional Repository

'You share, we take care!' - Taverne project

<https://www.openaccess.nl/en/you-share-we-take-care>

Otherwise as indicated in the copyright section: the publisher is the copyright holder of this work and the author uses the Dutch legislation to make this work public.



The effect of soil improvement and auxiliary rails at railway track transition zones

P. Chumyen^{a,*}, D.P. Connolly^a, P.K. Woodward^a, V. Markine^b

^a School of Civil Engineering, University of Leeds, LS2 9JT, UK

^b Delft University of Technology, Delft, the Netherlands

ARTICLE INFO

Keywords:

3D numerical railway model
Railway transition zones
Railroad auxiliary rail
Trackbed soil stiffness
Ballast-slab track

ABSTRACT

Railway track transition zones are areas where there is a sudden change in the track-ground structure. They include changes between ballasted and slab track, bridge approaches, and tunnel entry/exits. They are often the location of rapid track deterioration, and therefore this paper investigates the use of auxiliary rails and soil improvement to minimise train-track-ground dynamic effects. To do so, a 3D finite element model is developed using eight-node solid elements and a perfectly matched layer absorbing boundary condition. A moving train load is simulated using a sprung mass model to represent train-track interaction. After presenting the model, it is validated against field data collected on both a plain line and at a transition zone. Once validated, a sensitivity study is performed into auxiliary rails and soil improvement. It is found that auxiliary rails can improve the dynamic characteristics of the track across the transition, and that more widely spaced auxiliary rails provide greater benefit compared to closely spaced ones. Regarding soil improvement, a large benefit is found, and for the material properties under investigation, the effect of soil stiffening is greater than using auxiliary rails.

1. Introduction

Railway track transition zones are areas where there is a sudden change in the track-ground structure. They include changes between ballasted and slab track, bridge approaches, and tunnel entry/exits [1–3]. Changes can be related to the geometry of components and/or material properties. They impose differing stress fields across the transition, eventually leading to uneven track deterioration [4,5] reduced ride quality and the loss of passenger comfort [6,7]. Therefore, the maintenance incidence of track transitions can be up to eight times higher than plain line [8,9].

Track stiffness is defined as the load required to generate a unit of rail deflection [10] and depends on the track geometry and materials [11]. Differential track stiffness across a transition can cause problems that are exasperated by high train speeds and axle loads. Further, the quality of track material, particularly the compaction of ballast and subgrade [2, 4,12,13], including the presence of singular rail and wheel surface defect due to the structural discontinuity can generate high-level of track-ground vibration [14–17] which play important role in transition zone track degradation.

Numerical techniques such as the finite element method (FEM) can

be used to determine the dynamic response of railway tracks [18–22]. A suitable FEM approach depends on the required precision and the complexity of the problem [5]. 2D models can consider the discontinuities of track structure in either horizontal or longitudinal planes [23–26]. However, the real field geometries of track transition zones can be more complex and non-typical in both directions; for example, the embankment bridge approaches with the auxiliary rails representing the discontinuities in longitudinal and horizontal direction [27].

Alternatively, 3D models can overcome some 2D modelling limitations and have received significant attention, as discussed in Ref. [4]. Some transition models explicitly simulate the full track width and reduce the degree of freedom in the upper track via beam and spring-dashpot elements for the rail and rail pad [28–31]. A challenge with full track modelling is computational demand, especially when deep soils are included. This can be reduced by applying symmetric conditions for the horizontal track section, which assume that the load and stress distribution over the track is symmetrical [18,32]. Besides, modelling the soil by rigid support or spring element at the bottom of model cannot completely reproduce the soil properties and may result in unrealistic wave propagation [29,33]. Lastly, low absorption boundary conditions will allow outgoing waves to return to the structure, affecting

* Corresponding author.

E-mail address: ml16p3c@leeds.ac.uk (P. Chumyen).

<https://doi.org/10.1016/j.soildyn.2022.107200>

Received 3 December 2021; Received in revised form 31 January 2022; Accepted 11 February 2022

Available online 23 February 2022

0267-7261/© 2022 Elsevier Ltd. All rights reserved.

the numerical response [34]. Therefore, it is necessary to apply efficient methods to solve the problem of transient wave propagation. One of these is the perfectly matched layer (PML) [35–37].

Several studies proposed alternatives to improve transition zone performance by providing a smoother change in track stiffness between the softer and stiffer sides. The stiffness on the softer side can be improved by placing additional material and/or modifying the properties of the existing components. Some examples of solutions made on the softer side are adjustable rail fasteners [28], geosynthetic materials such as geogrid [38–40], geotextiles [41], hot-mix asphalt [42–44]; and modified wedge-shaped backfills using a combination of high modulus materials such as the cement bond granular (CBM), unbound granular (UGM) [45]. In contrast, some materials can be used to reduce the track stiffness on the stiffer side, such as baseplates [29], under sleeper pads [32,46], and ballast mats [33,47].

Another potential solution, that is a focus of this paper, is the application of auxiliary rails placed between the running rails [18,30,48]. Although only a limited number of studies have been performed related to this solution, potential benefits have been shown. For example, they have been shown to offer greater improvement in dynamic track behaviour than increasing sleeper length and using high modulus subgrade material [18]. Further, investigation into extra-long sleepers, lightweight sleepers and mixed solutions [49] has been performed, concluding that combining solutions with auxiliary rails and extra-long sleepers provides a smoother track behaviour change and increase passenger comfort.

Similar to auxiliary rails, few studies have investigated the effect of soil stiffness at transition zones [22]. This is important because it plays an important role in the track support condition. Further, in the presence of a track discontinuity, dynamic wave propagation is induced [50,51] which can be a contributor to degradation. The characteristics of this wave energy and its propagation are directly linked to the soil properties. Therefore, with the aim of better understanding this, this paper also investigates the effect of soil stiffness on dynamic transition zone behaviour.

To investigate both soil improvement and auxiliary rails, this paper describes the development of a 3D numerical model of a track transition zone. The model is established with symmetry around the track centreline and the absorbing boundary conditions are defined using perfectly matched layers. Then, a validation with field measurement data is performed to ensure the model can predict the dynamic response of transition zones. Finally, recommendations regarding the gauge of auxiliary rails and the soil improvement are presented.

2. Numerical model development

A finite element (FE) model is used to investigate dynamic behaviour at track transitions. The FE model developed is pre-processed using MATLAB and solved using LS-DYNA commercial software, with time-step of 4.94×10^{-6} s. Rather than use LS-DYNA's in-built keywords of *RAIL_TRACK and *RAIL_TRAIN, standard routines are used to maximise control over the simulation approach. The modelling parameters and methods are described in the following sections.

2.1. Track-soil modelling

The track structure and multi-layered soil are discretised into a series of elements using fully integrated eight-node solid hexahedral elements, with three translation degrees of freedom per node. The shape functions for the eight-node solid elements are given in Ref. [52]. Full coupling is assumed between the interfaces of each track component, including the ballasted and slab track transition, as shown in Fig. 1. Regarding the Cartesian coordinate system, X, Y and Z represent the longitudinal, vertical and horizontal directions, respectively. The element size is defined in accordance with the relationship between wavelength, frequency and shear wave speed [53,54].

The model is symmetric around the track centreline, with a single rail resting on discrete pads corresponding to the sleeper spacing. Since the rail has a complex geometry, it is modified to a rectangular section with an equivalent moment of inertia. The top of the sleepers is located at the same level as the ballast surface. Continuous solid elements are used to represent the concrete slab and supporting layers, such as the hydraulically bonded layer (HBL), the frost protection layer (FPL), and supporting multi-layered soils.

The material behaviour for all track components, including the soil, is isotropic and linear elastic. This assumes significant strain does not occur during train passage [55], meaning track displacements are limited to the elastic range of the stress-strain curve. The model formulation requires four material parameters: density, Young's modulus, Poisson's ratio and damping. In order to consider the rail pad stiffness in solid element modelling, the equivalent modulus (E_{qp}) is used considering the rail pad dimensions and Poisson's ratio, as shown in equation (1) from Ref. [56].

$$E_{qp} = k_{pad} \times \frac{H_{pad}}{W_{pad} \times L_{pad}} \times \frac{(1 + \nu_{pad})(1 - 2\nu_{pad})}{(1 - \nu_{pad})} \quad (1)$$

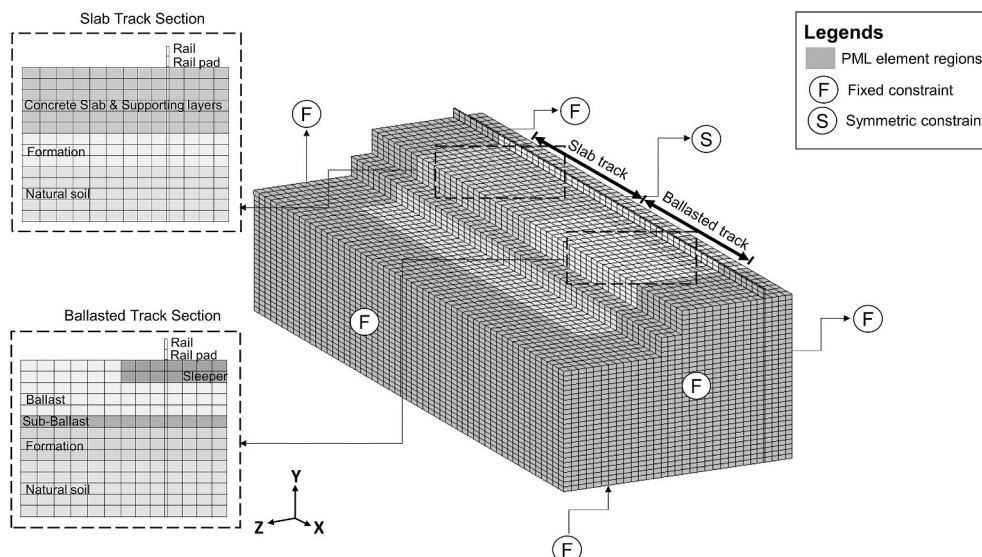


Fig. 1. Numerical modelling domain (truncated for viewability).

Where E denote Young's modulus (N/m^2), k is vertical stiffness (N/m), the dimensional parameters H , W , and L represent the thickness, width and length (m), respectively, and ν stands for the Poisson's Ratio.

For the domain boundary conditions, symmetry is implemented in the horizontal track section (XY -plane at $Z=0$), assuming the load and stress have a symmetric distribution along the track. Therefore, the constraints of rotation in the X and Y -axis, including the translation in the Z -axis, are defined. In addition, the PML approach is applied by placing additional eight solid elements through the depth next to the boundary of track components and soil [37]. The additional elements have mesh sizes and properties corresponding to the track domain. Moreover, the fixed constraints are implemented at the outer boundary of PML, as shown in Fig. 1.

2.2. Train-track interaction model

Since this study mainly focuses on track dynamics, other sources of dynamics, such as rail irregularity, are not considered. Instead, the vehicle-track coupling is simplified using a moving sprung mass model, as shown in Fig. 2.

The wheel mass (m_w) is applied at the top level of the spring, including the external load per wheel (f_{ext}) computed using the corresponding proportion of car bodies and bogies in equation (2).

$$f_{ext} = \left(\frac{m_{car}}{4} + \frac{m_{bogie}}{2} \right) \times g \quad (2)$$

Where m_{car} and m_{bogie} denote the mass of car body and bogie, and g stands for the gravitational acceleration, equal to 9.81 m/s^2 .

The Hertzian stiffness (k_h) is representative of the interaction between train and track, calculating by equation (3) [28,57]:

$$k_h = \sqrt[3]{\frac{3E_{rail}^2 f_s \sqrt{R_{wheel}} \times R_{railhead}}{2 \times (1 - \nu_{rail}^2)^2}} \quad (3)$$

Where (f_s) is the total static load per wheel (N), R represents the wheel radius (m) depending on the vehicle and curvature of rail (m). The input properties used throughout this paper were taken from Ref. [57].

The node (n_1) is always in contact with the top rail surface using the penalty-based approach. The contact definition identifies the top surfaces of rail and contact nodes (n_1) as the master and slave segments, respectively. The slave nodes are checked for penetration over the master surfaces at every time step. If penetrations occur, imaginary springs are placed between all penetrating nodes and contact surfaces.

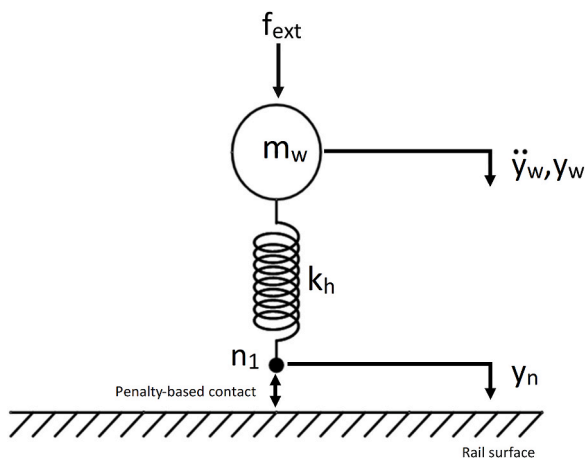


Fig. 2. Schematic of train-track interaction model for single axle.

2.3. Model simulation

The simulation process is composed of two phases: static and dynamic. The static analysis sets the initial conditions for the model, thus ensuring it is in static equilibrium, while the dynamic involves the moving load. The analysis applies the dynamic relaxation technique to initialise the domain to determine the initial conditions for the main simulation [52,58]. Therefore, the displacements throughout the domain at the starting point ($t=0$) are not equal to zero.

After computing the initial conditions, transient dynamic analysis is used to determine the track response to the moving loads. The classic equations of motion are expressed in equation (4) [59].

$$[M][\ddot{D}] + [C][\dot{D}] + [K][D] = [F] \quad (4)$$

Where $[M]$, $[C]$, and $[K]$ are the global mass, damping and stiffness matrices, while the vector $[F]$ represents the nodal forces. $[\ddot{D}]$, $[\dot{D}]$ and $[D]$ are the vectors of nodal accelerations, velocities and displacements, respectively, solved using central difference explicit time integration.

The material damping defined by $[C]$ is related to the mass and stiffness matrices using the Rayleigh damping coefficient [59]:

$$[C] = \alpha[M] + \beta[K] \quad (5)$$

Where α and β are the proportional constants with the unit of s^{-1} and s , respectively. Both values can be related to the damping ratio (ξ) and the circular frequency (ω) as [60,61]:

$$\xi = \frac{\alpha}{2\omega} + \frac{\omega\beta}{2} \quad (6)$$

For the moving load excitation, the matrix $[F]$ in equation (4) can be expressed as $[N]^T f_d$. The transposed shape function $[N]^T$ is null except for those relating to the nodal displacement of elements at the loading positions. f_d denotes the magnitude of moving force, which is computed using equation (7):

$$f_d = m_w \left(g - \ddot{y}_w \right) + k_h (y_w - y_n) + f_{ext} \quad (7)$$

Where the variables \ddot{y}_w and y_w represent vertical accelerations and displacements due to the motion of the wheel respectively, y_n is the vertical displacement of the contact node [62,63].

3. Model validation

The process to validate the proposed model is composed of two parts. Firstly, it is validated using a plain line case, to assess the general model accuracy. Then, a transition zone from ballasted to slab track is presented to show its ability to predict track behaviour at transition zones.

3.1. Plain line

The numerical results are compared with field tests performed on the Portuguese railway network [64]. The test site has dual ballasted tracks with straight alignment and a 1.668 m Iberian gauge. A constant element size of 0.2 m (equal the width of each sleeper) is modelled in the X -direction. For the Y and Z direction, the maximum element sizes are 0.25 and 0.20 respectively. The material properties and geometries for each track component are given in Table 1.

Regarding Table 1, the properties and geometries of rail are defined corresponding to UIC 60. Then, the equivalent rail pad modulus is computed using equation (1) and the field pad stiffness of 620 kN/mm. The spacing between sleepers is 0.6 m, and the Rayleigh damping coefficient of the rail pad is approximated using equation (5) by substituting the 22.5 kN/mm of viscous damping [66]. Also, the coefficients for sleeper, ballast, sub-ballast and all soil layers are estimated

Table 1
Summary of track geometry data and material properties for the plain line [65,66].

	Density (ρ) Unit: kg/m ³	Young modulus (E) Unit: MPa	Poisson Ratio (ν)	Rayleigh Damping Coefficient		Track geometry Unit: m		
				α Unit: 1/s	β Unit: s	Width (X-Axis)	Height (Y-Axis)	Length (Z-Axis)
Rail	7850	210,000	0.300	–	–	–	0.218	0.035
Rail pad	1000	5.86	0.494	5.00	3.75E-02	0.20	0.008	0.035
Sleeper	2500	30,000	0.200	1.67	5.30E-05	0.20	0.22	1.250 ^a
Ballast	1590	97	0.120	8.94	2.83E-04	–	0.55	1.700 ^a (top) 2.950 ^a (bottom)
Sub-Ballast	1900	212	0.200	6.14	1.95E-04	–	0.55	3.500 ^a
Soil Layer1	1900	110	0.4876	4.80	1.52E-04	–	1.50	4.000 ^a
Soil Layer2	1900	96	0.4929	4.80	1.52E-04	–	1.00	4.000 ^a
Soil Layer3	1900	164	0.4906	4.80	1.52E-04	–	1.00	4.000 ^a
Soil Layer4	1900	120	0.4953	4.80	1.52E-04	–	1.00	4.000 ^a
Soil Layer5	1900	145	0.4943	4.80	1.52E-04	–	0.50	4.000 ^a

^a Half-length due to the symmetry in Z-axis.

using equation (6) with the damping ratios of 1%, 6%, 4% and 3%, respectively [65].

The passage of the Alfa-Pendular train at 219 km/h is selected for model validation. The radius of wheel and railhead used to compute the Hertzian stiffness in equation (3) are 0.42 and 0.3 m, respectively [57]. To measure the vertical rail displacement, the set of Position sensitive detector (PSD) devices and laser sensors were installed in the descending track (direction from Porto to Lisbon) [64]. Fig. 3 illustrates the configuration of vertical loads per wheel given in kN.

The computed vertical rail displacements are presented in the time domain with a strong agreement between the fields measured data, as shown in Fig. 4.

3.2. Transition zones between ballasted-slab tracks

The numerical results are also validated against field test data on the Tehran-Karaj railway line in Iran [67]. Field data were collected at a transition zone from a slab track inside a tunnel to a ballasted track at the entrance/exit. The track consists of two lines with a gauge of 1.50 m. Two auxiliary rails with 18 m length are placed between the running rails on the ballasted track of the first line. The additional rails have cross-sections and properties identical to the main rail, and the distance between them is 0.5 m. The other parts of the line do not have any auxiliary rails. A constant element size of 0.3 m (equal the width of each sleeper) is modelled in the X-direction. For the Y and Z direction, the maximum element sizes are 0.12 and 0.20 respectively. The material properties and geometries for each track component are given in Table 2 and Table 3.

Regarding Tables 2 and 3, the rail properties and the modification of rail profile correspond to rail type UIC60. The longitudinal length (X-axis) is 60 m, consisting of a slab track 27 m long and a ballasted track 33 m long. The modulus of rail pad is adjusted from the field data with 180 kN/mm. The spacing between sleepers is 0.6 m. Further, the Rayleigh damping coefficients are approximated using 15 kN/mm viscous damping for the rail pad and a damping ratio of 3% for the remaining components [30].

The OBW 10 train manufactured by Plasser & Theurer is used to

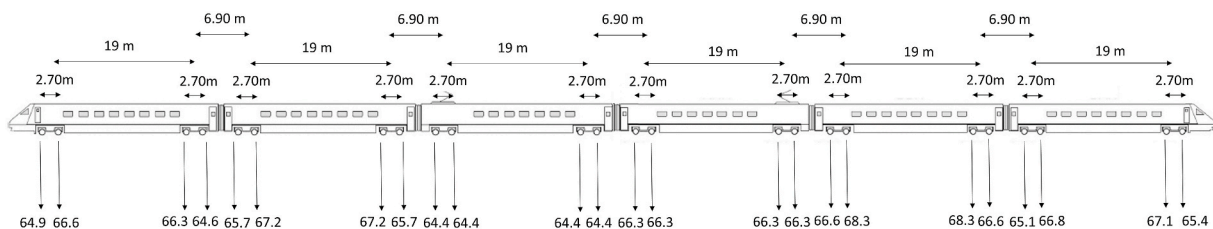


Fig. 3. Load configuration of the Alfa-Pendular train.

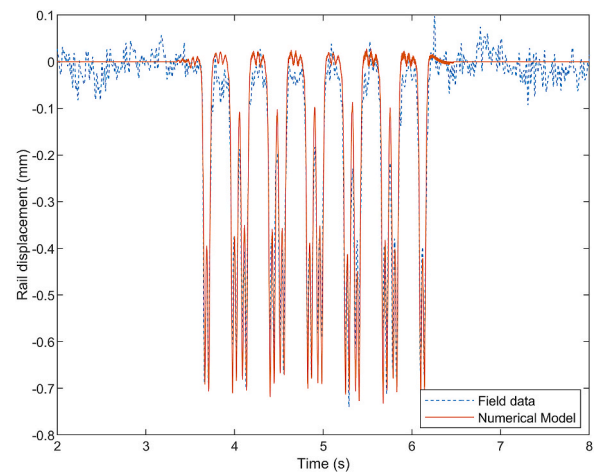


Fig. 4. Comparison of vertical rail displacements between Portuguese railway line data and numerical results.

simulate the test at 65 km/h, moving from the slab to ballasted track. The vehicle consists of two axles with the 130 and 100 kN wheel load, and the distance between them is 6.6 m. The Hertzian stiffness is computed using the same radius as in the previous validation. Fig. 5, Fig. 6, Fig. 7 and Fig. 8 present the transition zone model for the validation and the locations of Linear variable differential transformer (LVDT) sensors along the transition zones: at the slab track (sensor no.1) and at the ballasted track (sensor no.2 and 3) [30]. There is good agreement between the numerical results and field data for both cases of transition zones, hence validating the model, as shown in Fig. 9 and Fig. 10.

4. Model analysis

A sensitivity analysis was performed to provide an insight into

Table 2
Summary of track geometry data and material properties for common track structure of transition zones [30,67].

	Density (ρ) Unit: kg/m ³	Young modulus (E) Unit: MPa	Poisson Ratio (ν)	Rayleigh Damping Coefficient		Track geometry Unit: m		
				α	β	Width (X-Axis)	Height (Y-Axis)	Length (Z-Axis)
				Unit: 1/s	Unit: s			
Rail/Auxiliary rail	7850	210,000	0.300	–	–	–	0.218	0.035
Rail pad	1000	3.47	0.481	5.00	8.35E-02	0.30	0.008	0.035
Formation	1700	80	0.200	4.80	1.52E-04	–	0.36	3.500 ^a
Natural soil	1600	60	0.200	4.80	1.52E-04	–	2.00	4.500 ^a

^a Half-length due to the symmetry in Z-axis.

Table 3
Summary of track geometry data and material properties for ballasted and slab track component of transition zones [30,67].

	Density (ρ) Unit: kg/m ³	Young modulus (E) Unit: MPa	Poisson Ratio (ν)	Rayleigh Damping Coefficient		Track geometry Unit: m		
				α	β	Width (X-Axis)	Height (Y-Axis)	Length (Z-Axis)
				Unit: 1/s	Unit: s			
Sleeper	2500	50,000	0.200	–	–	0.30	0.24	1.300 ^a
Ballast	1800	130	0.200	4.80	1.52E-04	–	0.60	1.650 ^a (top) 2.950 ^a (bottom)
Sub-Ballast	1900	100	0.200	4.80	1.52E-04	–	0.12	3.500 ^a
Slab	2500	30,000	0.200	–	–	–	0.36	2.950 ^a
HBL	2200	10,000	0.100	4.80	1.52E-04	–	0.12	2.950 ^a
FPL	1900	110	0.200	4.80	1.52E-04	–	0.15	2.950 ^a
Prepared Subgrade	1900	100	0.200	4.80	1.52E-04	–	0.12	3.500 ^a

^a Half-length due to the symmetry in Z-axis.

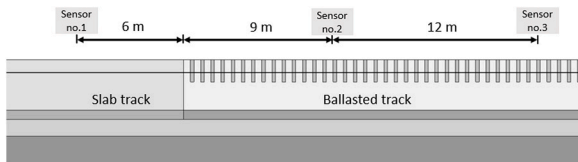


Fig. 5. Top view of transition model without auxiliary rail for validation.

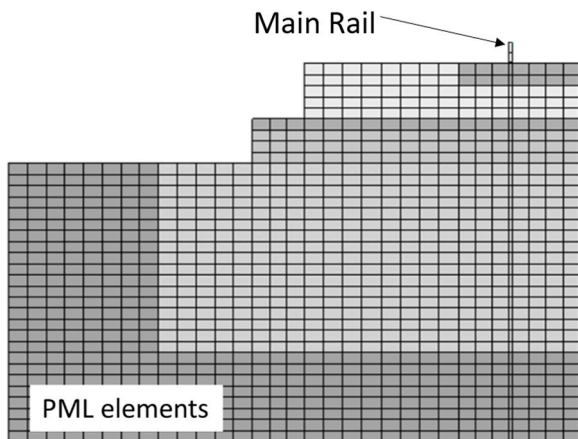


Fig. 6. Cross-Section of transition model without auxiliary rail for validation.

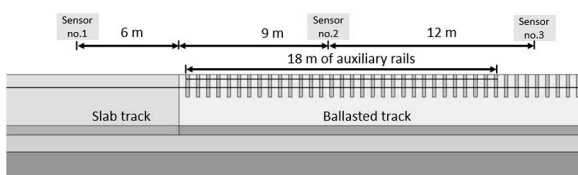


Fig. 7. Top view of transition model with auxiliary rail for validation.

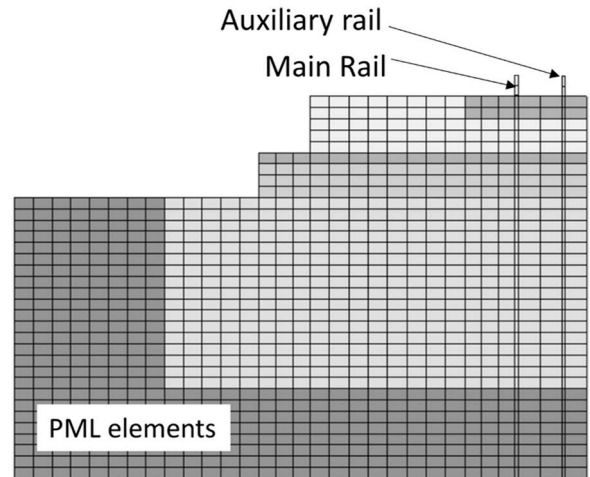


Fig. 8. Cross-section of transition model with auxiliary rail for validation.

auxiliary rail application and the impact of soil stiffness on transition zones. The simulation details and numerical results are presented in the following sections.

4.1. Effect of auxiliary rail gauge

The impact of four different gauges of auxiliary rail (0.3, 0.5, 0.8 and 1.2 m, as measured from track centre line), as shown in Fig. 11, are considered using the same track geometries and material properties as the validation case in section 3.2. The analysis consists of two parts: receptance behaviour and moving load response.

To understand the dynamic behaviour of the track transition zone with auxiliary rails, receptance tests are carried out on both sides of transition zones, by applying a unit force at the top of the rail. Two auxiliary rails with 18 m length each and a gauge of 0.5 m are placed on the ballasted track. The tests are performed and recorded at 10 m from

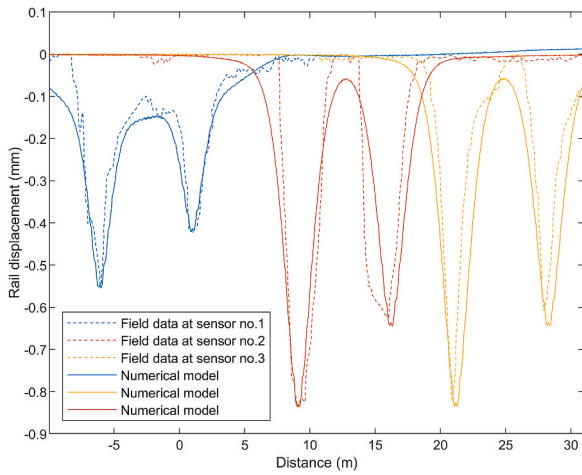


Fig. 9. Model validation: without an auxiliary rail.

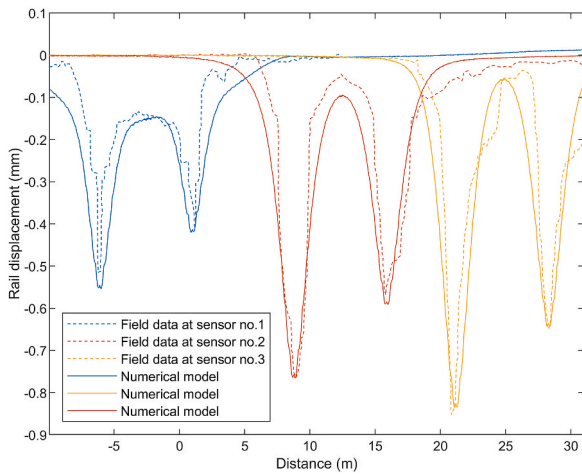


Fig. 10. Model validation: with an auxiliary rail.

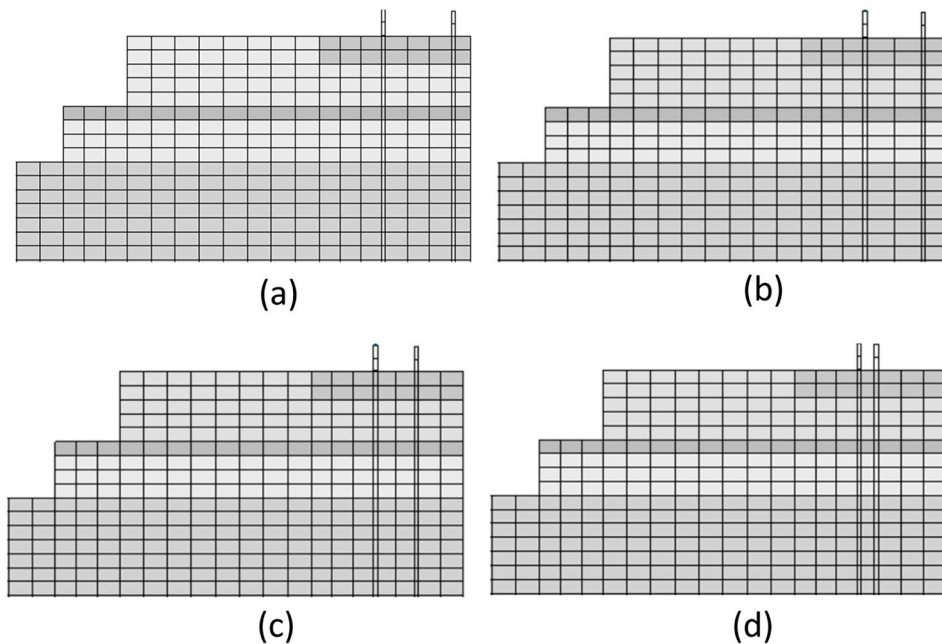


Fig. 11. Transition zones model with different auxiliary rail gauges: (a) 0.3 m, (b) 0.5 m, (c) 0.8 m, (d) 1.2 m, from track centre line.

the ballasted-slab track interface, as shown in Fig. 12. Fig. 13 presents the receptance responses of the transition zones with and without auxiliary rails at different locations, for the frequency range 0–100 Hz. It is seen that the ballasted track provides a higher rail receptance than the slab track, indicating the ballast track is less stiff over the majority of frequencies. This can be reduced by stiffening the track with the auxiliary rails. However, using the additional rails on the ballasted track becomes insignificant on the slab track’s receptance response because they are outside the zone of influence.

Next, the rail receptances for different ballasted track at the transition, with varying auxiliary rail gauges, are investigated, as shown in Fig. 14. The same track geometries and properties from the previous test are used. It can be seen that the wider gauge leads to a decrease in receptance at most frequencies, however the effect is minor.

Next, moving load simulations were performed, considering the same vehicle load as section 3.2 moving at 250 km/h. All track variables are the same as the receptance test.

Fig. 15 presents the maximum vertical rail displacement along the transition zones in the time domain. It is shown that using the auxiliary rail can decrease the differential rail displacement by 8% in the zone where it is placed. The difference is more pronounced compared to the receptance results. The benefit increases for wider gauges of auxiliary rail, with maximum benefit occurring at 1.2 m. However, note that the usage of auxiliary rails results in slightly increased displacement in the ballasted track after their termination. This is because of the new transition zone created due to the differing track stiffness’s either side of the auxiliary rail. Although the differential stiffness is small compared to that between ballast-slab, it should be considered during design to ensure it does not generated unexpected challenges.

The impact of different gauges on stress distribution is also investigated at two different locations; 5 and 10 m from ballasted-slab track

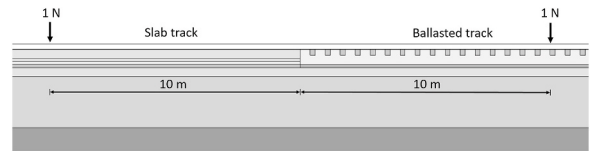


Fig. 12. Receptance impact locations.

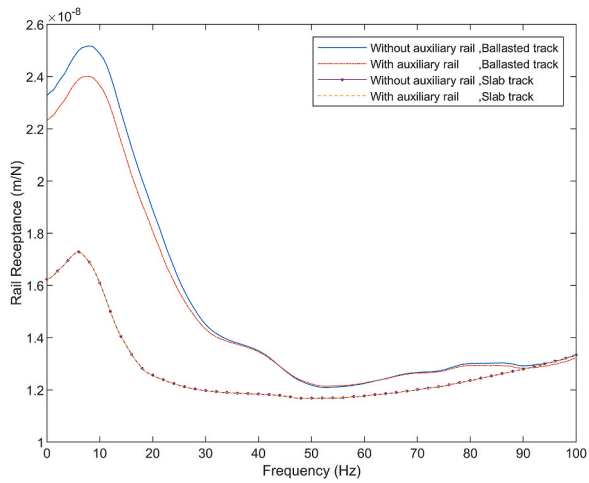


Fig. 13. Rail receptance obtained from slab and ballasted track of the transition zone with and without auxiliary rail.

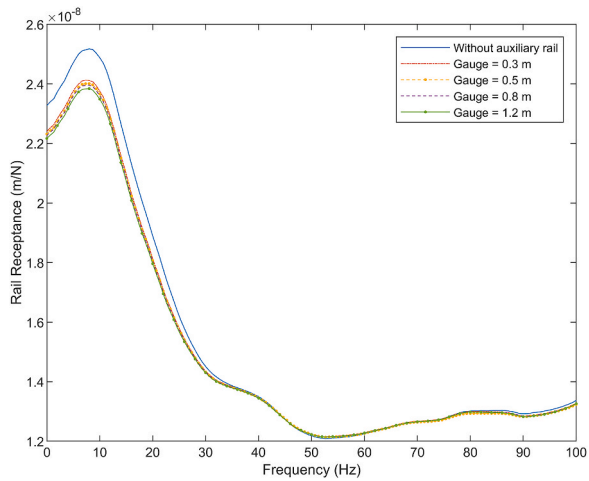


Fig. 14. Rail receptance obtained from the transition zone with a different gauge of auxiliary rail.

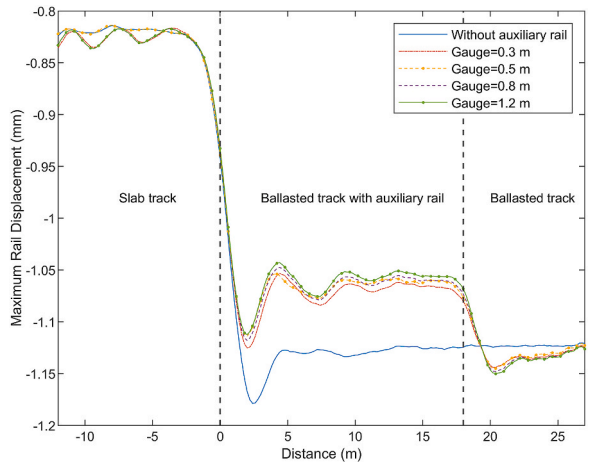


Fig. 15. Maximum rail displacement obtained from transition zones with a different gauge of auxiliary rail.

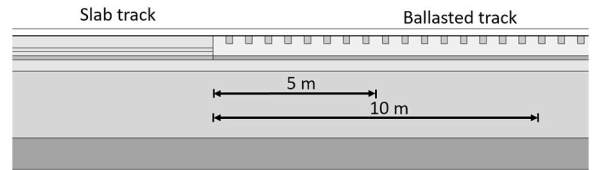


Fig. 16. Top view of stress measurement locations.

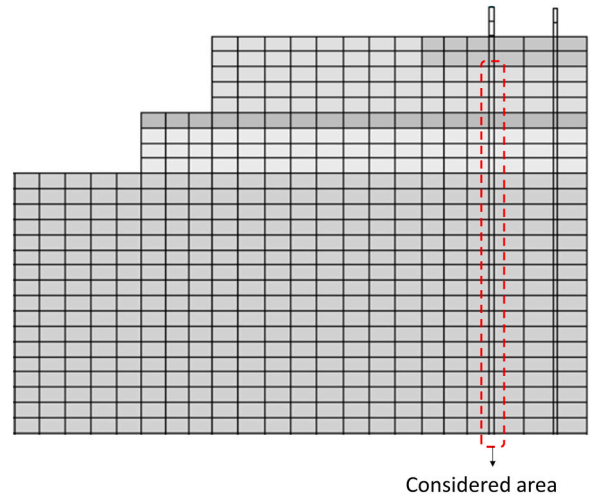


Fig. 17. Cross-section of stress measurement locations.

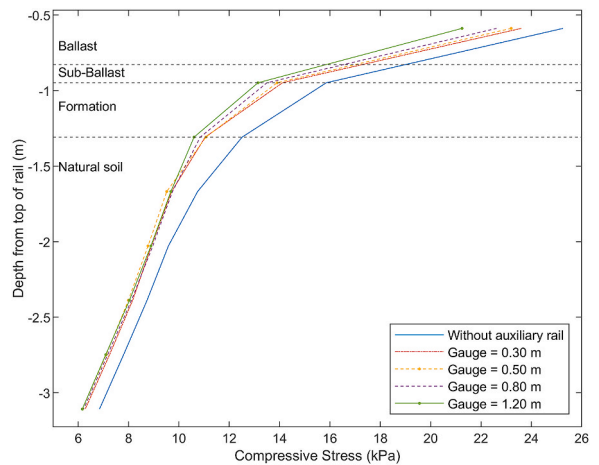


Fig. 18. Distribution of vertical compressive stress at 5 m from ballasted-slab track interface.

interface as shown in Fig. 16 and Fig. 17. Fig. 18 and Fig. 19 present the vertical distribution of compressive stress from ballast beneath the sleeper to natural soil at those locations. There is a similar trend at both measurement locations, indicating that the application of auxiliary rails decreases the compressive stress in the track and supporting soil. Similar to the previous analysis, the widest gauge provides the greatest reduction in the stress of upper layers (ballast, sub-ballast and formation). However, the effect diminishes with depth, and the impact is minimal in the soil.

4.2. Effect of soil stiffness

The impact of different soil stiffnesses on transition zone behaviour were investigated. To do so, soils with three different Young's modulus

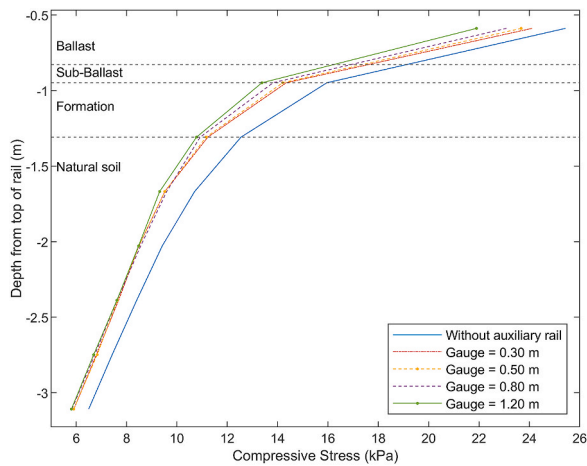


Fig. 19. Distribution of vertical compressive stress at 10 m from ballasted-slab track interface.

were analysed (50,100,150 MPa), each with a density of 2000 kg/m³ and Poisson’s ratio of 0.35 (the properties are different from Table 2). The track variables were kept the same as previously. The receptance tests are also performed at the same location as the previous section. The rail receptances in Fig. 20 show similar trends for both tracks. Increasing soil stiffness is seen to provide a reduction in rail receptance, particularly at low frequencies. Considering the peaks found in the <10 Hz range, the track receptance reduces by 22% and 31% when increasing to 100 and 150 MPa respectively. However, the impact is lower for the slab track where maximum reductions of 15% and 20% are achieved.

A similar trend is seen when repeating the moving load simulation from the previous section. Fig. 21 shows the maximum rail displacement response for the transition zones with different soil stiffnesses. The low stiffness soil of 50 MPa produces the highest rail displacements for both slab and ballasted tracks, resulting in a differential displacement of 45%. Similarly, the difference in displacement between both sides is reduced to 34% when increasing the soil stiffness to 100 MPa. Further, increasing the soil stiffness to 150 MPa provides a diminishing rate of improvement, with a differential deflection of 32%.

5. Conclusions

This paper presents a numerical analysis of dynamic track behaviour at transition zones, using the 3D finite element method. The transition model is developed using eight-node solid elements, using PML’s for

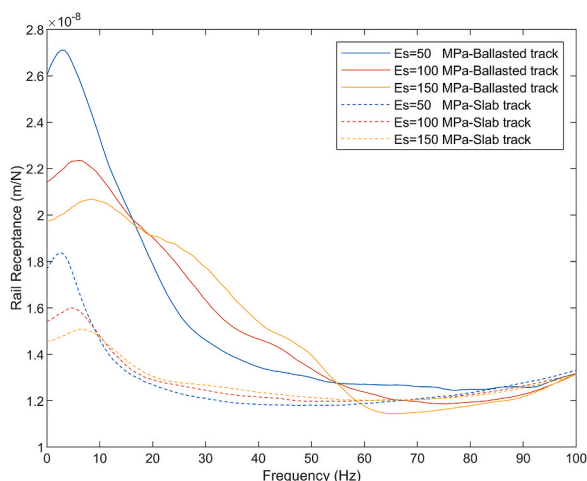


Fig. 20. Rail receptance for different soil stiffnesses.

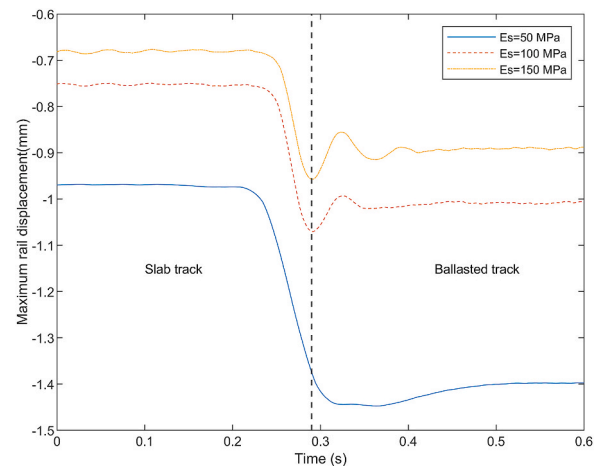


Fig. 21. Maximum rail displacement obtained from transition zones with a different soil stiffnesses.

absorbing boundary conditions. The moving load simulation employs a sprung mass model with Hertzian spring and penalty-based contact to represent train-track interaction.

The time-domain numerical results agree well with field track data collected on both plain line and transitions. After validation, sensitivity analyses of auxiliary rails and soil stiffness provide the following insights:

- Using two auxiliary rails can improve the dynamic characteristics of the track (i.e. receptance), differential rail displacement, and stress distribution in the ballasted track at a transition zone
- Placing auxiliary rails closer to the running rails, compared to a narrow placement, offers slightly improved dynamic performance
- When using auxiliary rails, care should be used to ensure any additional ‘mini’ transition zones introduced don’t give rise to unexpected dynamic behaviour
- Increasing soil stiffness improves differential dynamic rail displacements and receptance. The effect is more pronounced than using auxiliary rails.

CRediT authorship contribution statement

P. Chumyen: Methodology, Software, Analysis, Writing. D.P. Connolly: Conceptualization, Methodology, Resources, Writing, Supervision. P.K. Woodward: Supervision. V. Markine: Supervision, Writing.

Declaration of competing interest

The authors declare that they have no known competing financial interests or personal relationships that could have appeared to influence the work reported in this paper.

Acknowledgements

Leverhulme Trust (UK - PLP-2016-270), University of Leeds, Delft University of Technology.

References

[1] Li D, Hyslip J, Sussmann T, Chrismer S. Railway geotechnics. CRC Press Taylor&Francis Group; 2016.
 [2] Sañudo R, Dell’Olio L, Casado JA, Carrascal IA, Diego S. Track transitions in railways: a review. Constr Build Mater 2016;112:140–57.
 [3] Paixão A, Varandas JN, Fortunato E, Calçada R. Numerical simulations to improve the use of under sleeper pads at transition zones to railway bridges. Eng Struct 2018;164:169–82.

- [4] Indraratna B, Babar M, Ngo T, Gomes A, Kelly R. Improved performance of ballasted tracks at transition zones : a review of experimental and modelling approaches. *Transp Geotech* 2019;21.
- [5] Ramos A, Correia AG, Calçada R, Connolly DP. Ballastless railway track transition zones: an embankment to tunnel analysis. *Transp Geotech*; 2022.
- [6] Paixão A, Varandas JN, Fortunato E. Dynamic behavior in transition zones and long-term railway track performance. *Front Built Environ* 2021;7:1–16.
- [7] Li D, Davis D. Transition of railroad bridge approaches. *J Geotech Geoenviron* 2005;131(11):1392–8.
- [8] Hölischer P, Meijers P. Literature study of knowledge and experience of transition zones, Delft, The Netherlands. 2007.
- [9] Varandas JN, Hölischer P, Silva MAG. Dynamic behaviour of railway tracks on transition zones. *Comput Struct* 2011;89(13–14):1468–79.
- [10] Powrie W, Le Pen L. A guide to track stiffness. Southampton: University of Southampton; 2016.
- [11] Lamprea-pineda AC, Connolly DP, Hussein MFM. Beams on elastic foundations – a review of railway applications and solutions. *Transp Geotech* 2022;33.
- [12] Wang H, Markine V. Dynamic behaviour of the track in transition zones considering the differential settlement. *J Sound Vib* 2019;459.
- [13] Charoenwong C, Connolly DP, Woodward PK, Galvín P, Costa PA. Analytical forecasting of long-term railway track settlement. *Comput Geotech* 2022;143.
- [14] Kouroussis G, Connolly DP, Alexandrou G, Vogiatzis K. Railway ground vibrations induced by wheel and rail singular defects. *Veh Syst Dyn* 2015;53(10):1500–19.
- [15] Alexandrou G, Kouroussis G, Verlinden O. A comprehensive prediction model for vehicle/track/soil dynamic response due to wheel flats. *Proc Inst Mech Eng - Part F J Rail Rapid Transit* 2016;230(4):1088–104.
- [16] Germonpré M, Degrande G, Lombaert G. Periodic track model for the prediction of railway induced vibration due to parametric excitation. *Transp Geotech* 2018;17: 98–108.
- [17] Kouroussis G, Connolly DP, Vogiatzis K, Verlinden O. Modelling the environmental effects of railway vibrations from different types of rolling stock : a numerical study. *Shock Vib* 2015;2015.
- [18] Shahraki M, Warnakulasooriya C, Witt KJ. Numerical study of transition zone between ballasted and ballastless railway track. *Transp Geotech* 2015;3:58–67.
- [19] Varandas JN, Paixão A, Fortunato E, Hölischer P, Calçada R. Numerical modelling of railway bridge approaches: influence of soil non-linearity. *Int J Railw Technol* 2014;3.
- [20] Woodward PK, Laghrouche O, Mezher S, Connolly DP. Application of coupled train-track modelling of critical speeds for high-speed trains using three-dimensional non-linear finite elements. *Int J Railw Technol* 2015;1–35.
- [21] Connolly DP, Dong K, Costa PA, Soares P, Woodward PK. High speed railway ground dynamics: a multi-model analysis. *Int J Railw Technol* 2020;8:324–46.
- [22] Galvín P, Romero A, Dominguez J. Fully three-dimensional analysis of high-speed train – track – soil-structure dynamic interaction. *J Sound Vib* 2010;329:5147–63.
- [23] Paixão A, Fortunato E, Calçada R. Transition zones to railway bridges: track measurements and numerical modelling. *Eng Struct* 2014;80:435–43.
- [24] Punetha P, Maharjan K, Nimbalkar S. Finite element modeling of the dynamic response of critical zones in a ballasted railway track. *Front Built Environ* 2021;7: 1–11.
- [25] Sañudo R, Cerrada M, Alonso B, Olio L. Analysis of the influence of support positions in transition zones . A numerical analysis. *Constr Build Mater* 2017;145: 207–17.
- [26] Aggestam E, Nielsen JCO. Multi-objective optimisation of transition zones between slab track and ballasted track using a genetic algorithm. *J Sound Vib* 2019;446: 91–112.
- [27] Shan Y, Albers B, Savidis SA. Influence of different transition zones on the dynamic response of track-subgrade systems. *Comput Geotech* 2013;48:21–8.
- [28] Wang H, Markine V. Corrective countermeasure for track transition zones in railways : adjustable fastener. *Eng Struct* 2018;169:1–14.
- [29] Ngamkhanong C, Yan Q, Li T, Kaewunruen S. Dynamic train-track interactions over railway track stiffness transition zones using baseplate fastening systems. *Eng Fail Anal* 2020;118.
- [30] Heydari-Noghabi H, Varandas JN, Esmaili M, Zakeri JA. Investigating the influence of auxiliary rails on dynamic behavior of railway transition zone by a 3D train-track interaction model. *Lat Am J Solids Struct* 2017;14(11):2000–18.
- [31] Koch E, Hudacek P. 3D dynamic modeling of transition zones. *Zenodo* 2017;11(9): 1310–6.
- [32] Çati Y, Gökçeli S, Anil Ö, Korkmaz CS. Experimental and numerical investigation of usp for optimization of transition zone of railway. *Eng Struct* 2020;209.
- [33] Xin T, Ding Y, Wang P, Gao L. Application of rubber mats in transition zone between two different slab tracks in high-speed railway. *Constr Build Mater* 2020; 243.
- [34] Jia X, Liu X, Li G. A non-reflective boundary model applied to finite element analysis of railway track structure. In: Proceedings of the asia-pacific conference on intelligent medical 2018 & international conference on transportation and traffic engineering 2018. New York, United States: Association for Computing Machinery; 2018. p. 15–9.
- [35] Barbosa J, Park J, Kausel E. Perfectly matched layers in the thin layer method. *Comput Methods Appl Mech Eng* 2012;217–220:262–74.
- [36] Connolly DP, Giannopoulos A, Forde MC. A higher order perfectly matched layer formulation for finite-difference time-domain seismic wave modeling. *Geophysics* 2015.
- [37] Basu U. Explicit finite element perfectly matched layer for transient three-dimensional elastic waves. *Int J Numer Methods Eng* 2009;151–76.
- [38] Connolly DP, Yu HS. A shakedown limit calculation method for geogrid reinforced soils under moving loads. *Geotext Geomembr* 2021;49:688–96.
- [39] Indraratna B, Qi Y, Ngo TN, Rujikiatkamjorn C. Use of geogrids and recycled rubber in railroad infrastructure for enhanced performance. *Geosciences* 2019.
- [40] Yu Z, Woodward PK, Laghrouche O, Connolly DP. True triaxial testing of geogrid for high speed railways. *Transp Geotech* 2019;20.
- [41] Arulrajah A, Bo MW, Abdullah A, Leong M. Geosynthetic applications in high-speed railways : a case study. *Proc Inst Civ Eng : Ground Improv* 2015;168.
- [42] Palomo ML, Barcelo FR, Llarío FR, Herra JR. Effect of vehicle speed on the dynamics of track transitions. *Vib Control* 2018.
- [43] Setiawan DM. Worldwide hot mix asphalt layer application and scrap rubber and bitumen emulsion studies on railway track-bed. *Semesta Teknika* 2018.
- [44] Yu Z, Connolly DP, Woodward PK, Laghrouche O. Settlement behaviour of hybrid asphalt-ballast railway tracks. *Constr Build Mater* 2019;208:808–17.
- [45] Paixão A, Fortunato E, Calçada R. Design and construction of backfills for railway track transition zones. In: *Proc Inst Mech Eng - Part F J Rail Rapid Transit*; 2015.
- [46] Paixão A, Nuno J, Fortunato E, Calçada R. Numerical simulations to improve the use of under sleeper pads at transition zones to railway bridges. *Eng Struct* 2018; 164:169–82.
- [47] Lima ADO, Dersch MS, Qian Y, Tutumluer E, Edwards JR. Laboratory evaluation of under-ballast mat effectiveness to mitigate differential movement problem in railway transition zones. In: *Bearing capacity of roads, railways and airfields*. CRC Press; 2017.
- [48] Esmaili M, Kamali M, Heydari-noghabi H. Numerical investigation of railway transition zones stiffened with auxiliary rails. *Proceedings of the Institution of Civil Engineers - Transport*. ICE Publishing; 2017.
- [49] Sañudo R, Markine V, Pombo J. Study on different solutions to reduce the dynamic impacts in transition zones for high-speed rail. *J Theor Appl Vib Acoust* 2018;3(2): 199–222.
- [50] Dong K, Connolly DP, Laghrouche O, Woodward PK, Costa PA. The stiffening of soft soils on railway lines. *Transp Geotech* 2018;17:178–91.
- [51] Connolly DP, Costa PA. Geodynamics of very high speed transport systems. *Soil Dyn Earthq Eng* 2020;130.
- [52] Hallquist JO. *LS-DYNA Theory Manual*. California: Livermore Software Technology Corporation; 2006.
- [53] Shih JY, Thompson DJ, Zervos A. The effect of boundary conditions , model size and damping models in the finite element modelling of a moving load on a track/ground system. *Soil Dyn Earthq Eng* 2016;89:12–27.
- [54] Kouroussis G, Van Parys L, Conti C, Verlinden O. Using three-dimensional finite element analysis in time domain to model railway-induced ground vibrations. *Adv Eng Softw* 2014;70:63–76.
- [55] Dong K, Connolly DP, Laghrouche O, Woodward PK, Costa PA. Non-linear soil behaviour on high speed rail lines. *Comput Geotech* 2019;112:302–18.
- [56] Matias S. Numerical modeling and design of slab tracks - Comparison with ballasted tracks. Instituto Superior Técnico, University of Lisbon; 2014.
- [57] Mosleh A, Costa PA, Calçada R. A new strategy to estimate static loads for the dynamic weighing in motion of railway vehicles. *Proc Inst Mech Eng - Part F J Rail Rapid Transit* 2020;234(2):183–200.
- [58] Pajand MR, Hakkak MT. Nonlinear Analysis of truss structures using dynamic relaxation. *Int J Eng* 2006;19(1).
- [59] Lui GR, Quek SS. *The finite element method : a practical course*. Elsevier Ltd; 2003.
- [60] Cruz C, Miranda E. A critical review of the Rayleigh damping model. In: *Proceedings of the 16th world conference on earthquake engineering*; 2018.
- [61] Alipour A, Zareian F. Study Rayleigh damping in structures ; uncertainties and treatments. In: *Proceedings of the 14th world conference on earthquake engineering*; 2008.
- [62] Esveld C. *Modern railway track*, second. Delft, The Netherlands. 2001.
- [63] Lin YH, Trethewey MW. Finite element to analysis of elastic beams subjected to moving load dynamic beams. *J Sound Vib* 1990;323–42.
- [64] Correia N, Colaço A, Costa PA, Calçada R. Experimental analysis of track-ground vibrations on a stretch of the Portuguese railway network. *Soil Dyn Earthq Eng* 2016;90:358–80.
- [65] Ruiz JF, Costa PA, Calçada R, Medina LE, Colaço A. Study of ground vibrations induced by railway traffic in a 3D FEM model formulated in the time domain : experimental validation. *Struct Infrastruct Eng* 2017;13(5):652–64.
- [66] Costa PA, Cardoso S. Experimental validation of a 2.5D FEM-BEM model for the assessment of vibrations induced by traffic. In: *Proceeding of the 3rd computational methods in structural dynamics and earthquake engineering*. National Technical University of Athens; 2011.
- [67] Heydari H, Zakeri JA, Esmaili M. Field study using additional rails and an approach slab as a transition zone from slab track to the ballasted track. In: *Proc Inst Mech Eng - Part F J Rail Rapid Transit*; 2017.